Design of a surface-mounted PM motor for improved flux weakening performance

Article:

Design of a Surface-Mounted PM Motor for Improved Flux Weakening Performance

Stavros Pastellides, Stiaan Gerber, Rong-Jie Wang and Maarten J. Kamper

Abstract—In this paper a surface-mounted permanent magnet motor with a distributed overlapping winding is designed for a light electric vehicle. The motor specifications are derived from the vehicle physics model where the operating points are determined. A theoretical understanding is developed of how to improve the motor's speed range through changes in the equivalent circuit parameters and the resulting effect on the geometry. It is shown that with an increase in inverter size, a more cost effective motor design is achievable. An optimisation is conducted for the specified motor to find the most cost effective design based on a selected inverter size. The optimised design is shown to withstand a short-circuit condition without magnet degradation. Further the optimisation shows that, for a conventional surface-mounted permanent magnet motor, a wide flux weakening range can be realised by increasing the slot-leakage inductance.

Index Terms—Design optimisation, electric vehicles, flux weakening, permanent magnet motors, surface-mounted, traction motors

I. INTRODUCTION

Globally, light electric vehicles (LEV) are increasingly used in both urban environments, factories and warehouse facilities. Comparing with internal combustion engines (ICE), electric motors are more energy efficient and their torque-speed characteristics are better suited for the requirements of the specified applications. Although different electric motor technologies are available for electric vehicle (EV) applications, permanent magnet (PM) machines are often considered in the implementation of EVs [1]–[5]. Among them, the surface-mounted PM (SPM) and interior PM (IPM) machines are the most common topologies.

Whilst the SPM motor has a better PM utilization factor than its IPM counterpart [6], [7], the relatively narrow constant power speed range (CPSR) and demagnetization risks often pose design challenges. To improve the flux weakening performance of SPMs, fractional-slot non-overlap winding (FSNOW) configurations have been proposed in literature [8]–[11].

Generally, the FSNOW has the potential benefits of possessing an increased magnetising inductance and the improved flux weakening performance. Furthermore the end-winding length is significantly shorter when compared with

Fig. 1. The battery powered campus security vehicle.

overlap windings, thus, resulting in lower losses and easier manufacturability. However, the magnetic fields of FSNOW machines have rich space harmonics. These sub- and high harmonics have negative impact on the machine performance causing localized core saturation, excessive iron and PM losses [12], which are the main disadvantages of FSNOWs.

In this paper a SPM motor with conventional distributed overlap winding is designed for a battery powered campus security vehicle. To improve on the flux weakening performance, the SPM motor parameters relating to the CPSR were analysed, which shows that the conventional SPM motor can be designed with a wide CPSR by increasing stator leakage inductances.

II. TRACTION MOTOR AND LEV

This study focuses on the design of a traction motor for a campus security vehicle (shown in Fig. 1). An analysis using the basic vehicle physics model, which incorporates the vehicles resistances and acceleration, is first conducted for the LEV [13], [14]. The design specifications of the drive-train components are determined based on the required vehicle performance, summarised in Table I. For this motor, the required output power is 3 kW, and the maximum speed of the vehicle is 50 km/h. The drive train of the vehicle operates through a back axle drive, with the motor being coupled to a magnetic gear (MG) as shown in Fig. 2.
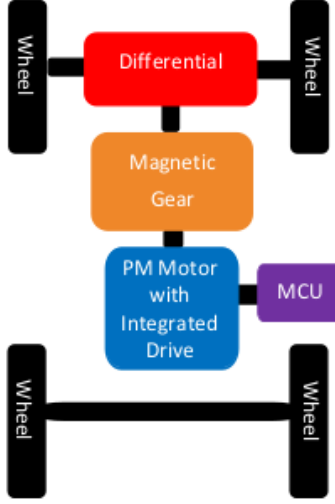
Fig. 2. Proposed drive-train topology of the LEV.

TABLE I
THE SPECIFICATIONS OF THE LEV.

Parameter	Value
Wheel radius (m)	0.299
Frontal area (m^2)	2.5
Aerodynamic drag coefficient	0.3
Rolling resistance coefficient	0.013
Grading percentage (%)	0
Vehicle mass (kg)	1000
Maximum vehicle speed (km/h)	50
MG Gear ratio	11:1
Maximum MG torque (Nm)	254

TABLE II
DESIGN SPECIFICATIONS OF THE SPM MOTOR.

| Parameters	Value
Outer radius (mm)	106
Shaft size (Diameter) (mm)	30
Nominal power (kW)	3
Maximum voltage (V_{max}) (V)	48
Nominal current (I_S) (A)	40
Peak loss (W)	300
Number of slots	36
Number of pole pairs	4
Air-gap length (mm)	1
Slot fill factor	0.35
Base motor speed (r/min)	1500
Max motor speed (r/min)	5000
Motor torque at base speed (Nm)	19.1
Motor torque at maximum speed (Nm)	5.73
CPSR ratio	3.33
Winding temperature (°C)	120
PM remnant flux density (@80°C) (T)	1.39
PM recoil permeability	1.05
Demagnetization knee point (T)	0.2
PM material and grade	NdFeB N48H
Core material	M19_26G
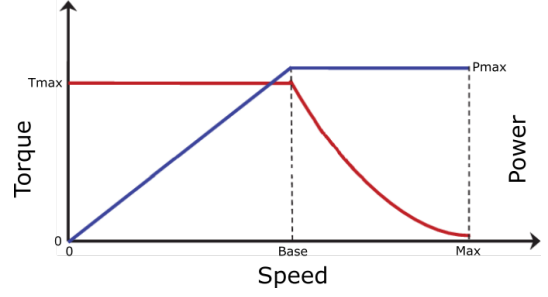
Fig. 3. Torque / power-speed curve of motor.

A. Proposed Motor Design

The design specifications for the motor is given in Table II. The MG utilised for this study has an outer radius of 106 mm and shaft size of 30 mm. To allow for easier coupling and housing of both components, the maximum motor outer radius is also constrained to the same value.

As shown in a previous study [6], the 36-slot and 8-pole PM motor design was chosen for this study. The power of the motor and the inverter requirements are set by keeping the maximum voltage V_{max} and armature current I_S at nominal values. The apparent power of the inverter is set to be:

$$S = \sqrt{3}V_{max}I_S \quad \text{(VA)} \tag{1}$$

By specifying the winding temperature to be 120°C and setting the maximum overall losses to be 300 W, the thermal loading and efficiency of the motor is inherently constrained.

The grade and material of magnets selected for this study is NdFeB N48H operating at 80°C. The "knee" point of the demagnetisation curve for these magnets at 80° is found at 0.2 T. In order to mitigate the risk of demagnetization, especially during flux weakening operation, a constraint is set for a demagnetization margin. This margin ensures the flux density of the magnets are above this point.

III. IMPROVING THE CPSR OF SPM MOTOR

Typical torque/power-speed characteristics of a traction motors are shown in Fig. 3, where two distinct operation areas are defined, namely, the constant torque and constant power regions. To determine the motor's performance in these regions, the steady-state voltage and torque equations of a PM synchronous motor are expressed as [2], [15], [16]:

$$v_d = R_s i_d - \omega_e L_q i_q \tag{2}$$

$$v_q = R_s i_q + \omega_e(L_d i_d + \lambda_{PM}) \tag{3}$$

$$T_e = \frac{3}{2}p[\lambda_{PM} + (L_d - L_q)i_d]i_q \tag{4}$$

where v_d, v_q, i_d, i_q, L_d, L_q are the d- and q-axis voltages, currents and inductances respectively, R_s is the phase resistance, λ_{PM} is the PM's flux-linkage, ω_e is the electrical rotational speed, p is the number of pole pairs and T_e is the electromagnetic torque.
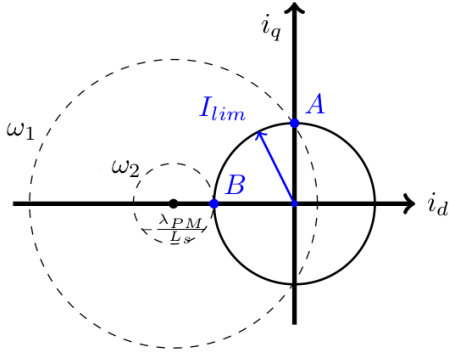
Fig. 4. Current / voltage limit for a SPM in dq-current plane.

For any operating point of the motor, the current and voltage limits, which is constrained by the inverter rating, should not be exceeded. These constraint limits can be expressed as:

$$V_{max}^2 \geq (v_d^2 + v_q^2) \tag{5}$$

$$I_{lim}^2 \geq (i_d^2 + i_q^2) \tag{6}$$

From (6), a current limit circle with radius I_s and a centre at the origin can be formulated within the dq-current plane.

A. CPSR Related Parameters of a SPM Motor

It can be assumed for a SPM motor that $L_d = L_q = L_s$ [2], [8], [13], [16], where L_s is the synchronous inductance. Further, by assuming a negligible phase resistance, (2), (3) and (4) can be simplified as:

$$v_d = -\omega_e L_s i_q \tag{7}$$

$$v_q = \omega_e(L_s i_d + \lambda_{PM}) \tag{8}$$

$$T_e = \frac{3}{2} p \lambda_{PM} i_q \tag{9}$$

and by substituting (7) and (8) into (5), expression (5) can be rewritten as:

$$\left(\frac{V_{max}}{\omega_e L_s}\right)^2 \geq i_q^2 + \left(i_d + \frac{\lambda_{PM}}{L_s}\right)^2 \tag{10}$$

which shows that the voltage is constrained by a circle with a centre point of $(0, -\frac{\lambda_{PM}}{L_s})$ and a radius of $\frac{V_{max}}{\omega_e L_s}$. The current and voltage limit regions are shown in Fig. 4 in the dq-current plane. At the base speed, shown as point A in Fig. 4, both circles intersect on the q-axis, where i_q is at the current limit subjecting also to the voltage constraint. From (10), the base speed can be expressed as:

$$\omega_b = \frac{V_{max}}{\sqrt{(L_s I_{lim})^2 + \lambda_{PM}^2}} \tag{11}$$

Points A and B in Fig. 4, refer to the operating regions for the SPM. At Point A, the motor operates at the constant torque region, whereas between points A to B is the flux

weakening operation range. For a finite speed motor drive, the maximum speed occurs where both constraint circles meet at a single point [17]. The maximum speed is thus:

$$\omega_{max} = \frac{V_{max}}{\lambda_{PM} - L_s I_{lim}} \tag{12}$$

From (11) and (12), a CPSR factor (K_{CPSR}) based on the maximum to base speed ratio can be defined as [18]:

$$K_{CPSR} = \frac{\omega_{max}}{\omega_b} = \frac{\sqrt{(L_s I_{lim})^2 + \lambda_{PM}^2}}{\lambda_{PM} - L_s I_{lim}} \tag{13}$$

Further, the characteristic current of a SPM is defined as [9]:

$$I_n = \frac{\lambda_{PM}}{L_s} \tag{14}$$

By decreasing I_n, which in turn shifts the voltage limit circles in Fig. 4 to the right, an increase of CPSR can be achieved. As seen from (13) and (14), the PM flux linkage has an effect on the CPSR, however, by altering λ_{PM}, the torque capability of the motor is also affected. Alternatively, the synchronous inductance of the motor can be increased to reduce I_n and thus improve the CPSR of the motor [9]. It can be seen that the ideal flux weakening occurs when the the characteristic current I_n equals the rated current I_{lim}, however, this will lead to the demagnetisation of the PMs.

B. Synchronous Inductance Components

The synchronous inductance of a PM motor can be expressed as [19]:

$$L_s = L_m + L_L \tag{15}$$

where L_m is the magnetising inductance and L_L is the leakage inductance. The L_m can be further written as:

$$L_m = \mu_0 \frac{2m\tau_p}{\pi^2 p \delta_{ef}} l'(k_{ws1} N_s)^2 \tag{16}$$

where μ_0 is the permeability of air, m is the number of phases, τ_p is the pole pitch, δ_{ef} is the effective air-gap, l' is the length of the machine and $k_{ws1} N_s$ is the effective turns of the winding with regards to the winding factor.

The leakage inductance has several components, which can be expressed as:

$$L_L = L_\sigma + L_e + L_h \tag{17}$$

where L_σ is the slot leakage inductance, L_e is the end-winding leakage inductances and L_h is the air-gap harmonic leakage inductance. The slot leakage inductance can be defined by the equation below [19]:

$$L_\sigma = \frac{4m}{Q} \mu_0 l' N^2 \sigma_u \tag{18}$$
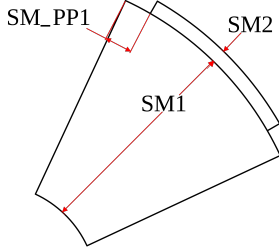
where Q is the number of slots and σ_u is the permeance factor. For a double-layer winding, σ_u can be calculated as:

$$\sigma_u = k_1 \frac{S_3}{3S_6} + k_2 \left(\frac{S_1}{S_5} + \frac{S_7}{S_6 - S_5} ln \frac{S_6}{S_5}\right) \tag{19}$$

where k_1 and k_2 are the short pitching factors [19]. The stator parameters in (19) are shown in Fig. 5.
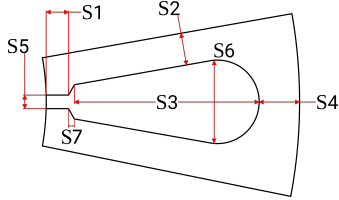
(a) Stator slot dimension variables.

(b) Rotor dimension variables.

Fig. 5. Motor geometry design variables for optimisation.

TABLE III
COSTS OF MATERIALS USED IN THE OPTIMISATION.

Material	Cost (USD/kg)
Permanent magnets (NdFeB)	50
Electric steel lamination	2
Copper	6.67

IV. OPTIMISATION FORMULATION

Optimising electrical machines for traction applications can be quite complicated since different performance characteristics are required at different operational speeds. The two-point optimisation strategy described in [6] is implemented in this study. These points were specified from the torque speed specifications in Table II, i.e. base speed and maximum speed. By analysing only these two points and ensuring they are within the inverter requirements, the compliance of the motor performance over the full operating speed range is inherently ensured.

A. Optimisation algorithm

The optimisation method implemented for this study, was the sequential least squares programming algorithm (SLSQP) [20], which is a gradient-based optimisation method. The SLSQP minimises a single objective function of multiple variables, subjecting to some equality and inequality constraints.

B. Optimisation problem

The optimisation simulations were conducted using an in-house 2D finite element (FE) package. By using the two operating points, the optimisation problem is formulated as:

Minimise: $F(\mathbf{X}) = C_{\text{total}}$

Subject to:
$T_1 \geq 19.1 \, \text{Nm}$ $\qquad$ $T_2 \geq 5.73 \, \text{Nm}$
$V_{max1} \leq 48 \, \text{V}$ $\qquad$ $V_{max2} \leq 48 \, \text{V}$
$I_{\phi1} \leq 40 \, \text{A}$ $\qquad$ $I_{\phi2} \leq 40 \, \text{A}$
$P_{\text{loss1}} \leq 300 \, \text{W}$ $\qquad$ $P_{\text{loss2}} \leq 300 \, \text{W}$
$B_{MM1} \geq 0.05 \, \text{T}$ $\qquad$ $B_{MM2} \geq 0.05 \, \text{T}$

where $\mathbf{X}$ represents the vector of design variables including the geometric variables as shown in Fig. 5, dq-currents for

each operating point and the coil turns of the machine. C_{total} is the total cost of the machine. The costs of the constituent materials of a PM machine are given in Table III [21]. T_1 and T_2 are the minimum required torques, V_{max1} and V_{max2} are the maximum voltage limits, $I_{\phi1}$ and $I_{\phi2}$ are the maximum allowable phase currents, $P_{\text{loss 1}}$ and $P_{\text{loss 2}}$ are the maximum allowable total losses, and B_{MM1} and B_{MM2} are the demagnetisation margins of magnets, for design point 1 and 2, respectively.

Each design variable utilised in the optimisation has a significant influence on the motor performance for the specified operating point. By tuning the dq-current design variables, the optimal current angle is inherently determined for the specified point and hence the optimal torque. Further, by adjusting the geometric parameters, the magnetising and slot leakage inductances are changed, which has an impact on the flux weakening performance of the motor. However, with the adjustment of these parameters, the cost objective function is also affected. The optimisation is required to determine the optimal weight for each material while ensuring the operating point specifications are met.

C. Inverter size versus motor cost

It was found during the initial optimisation process, that an adjustment of the inverter size has a significant influence on the total cost of the motor design. The relationship between the inverter size and the cost of the SPM motor is shown in Fig. 6, which was realised by performing multiple design optimisations based on a range of inverter ratings. The increase in inverter size is realised by increasing the maximum current while maintaining the same maximum voltage of 48 V. It is clear that the cost of the motor falls sharply with the increase of inverter rating.

It is generally difficult to find an exact unit cost per kVA rating for inverters. This is due to the number of technologies and topologies available which has costing differences. Nonetheless, it is estimated for this design, that as the inverter rating increases from 3.4 kVA to 4.1 kVA, the cost increase will be minor relative to the savings of the motor.

From Fig. 6, the smallest inverter size possible for the set specifications is shown to be 3.4 kVA, with a total motor cost of 94 USD. From a system perspective, it is advised that an inverter with a rating of approximately 3.7 kVA is selected for this application. The motor cost is thus reduced to approximately 50 USD.

V. PERFORMANCE ANALYSIS

In this section, the optimisation results and performance characteristics of the designed SPM motor are discussed in
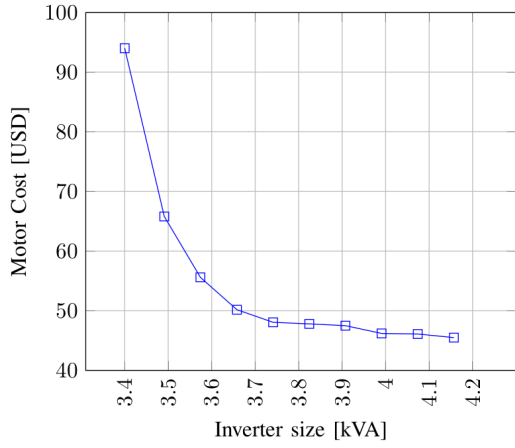
Fig. 6. Motor cost as a function of inverter size.

Fig. 8. Cross-section of optimised short-circuit tolerant surface-mounted motor.

TABLE IV
MOTOR DESIGN PARAMETERS.

Parameter	Initial Optimum Design	Final Design
SM_PP1	0.728	0.756
$SM1$ (mm)	42.27	31.03
$SM2$ (mm)	1.29	1.8
$S1$ (mm)	9.82	15.56
$S2$ (mm)	3.34	2.89
$S3$ (mm)	24.05	25.16
$S4$ (mm)	10.798	13.72
$S5$ (mm)	2	2
$S6$ (mm)	9.09	9.44
$S7$ (mm)	1.735	2.7
Stack length (mm)	57.34	57.68
Number of turns per coil	4	4

TABLE V
OPERATING POINT RESULTS FOR OPTIMISED SHORT-CIRCUIT TOLERANT
DESIGN.

Parameter	Optimised Design	
Operating point $\rightarrow$	$\omega_{\mathrm{b}} = 1500\,\mathrm{r/min}$	$\omega_{\max} = 5000\,\mathrm{r/min}$
Torque (Nm)	19.1	5.73
$V_{\max}$ (V)	48	48
I_{rms} (A)	44	44
Copper losses (W)	234	234
Core losses (W)	28.75	47
Magnet losses (W)	8.75	16
Demagnetisation margin (T)	0.136	0.225
Constant power speed range	1	3.33
Demagnetisation margin (T) (dynamic short-circuit state)	0.018	0.103
Short-circuit current (A)	74.08	64.52

detail. An initial optimised design is first shown, followed by a refined optimised design that is able to withstand a short-circuit condition without permanent demagnetisation. For validation purpose, the designs are determined by using the in-house FE package and have been analysed by the ANSYS-Maxwell commercial package.

A. *Operating point results*

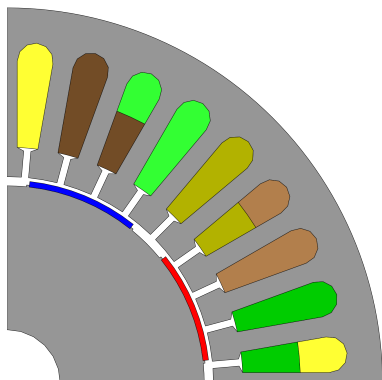Figure 7 shows the initial optimised SPM motor design for the inverter size of 3.7 kVA, with the geometric design

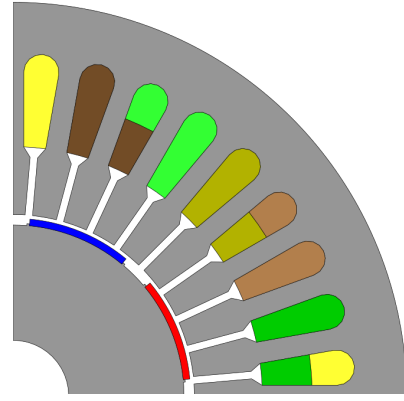Fig. 7. Cross-section of initial optimised surface-mounted motor.

parameters summarised in Table IV. The design was validated at both base and maximum speed operating points, which confirms that the initial optimum design satisfies all the design specifications. To assess the short-circuit withstand capability of the initial design, it is tested under a dynamic short-circuit condition, as described in [22]. Unfortunately, the initial optimum design suffers severe demagnetisation risk at either operating point. To mitigate this phenomenon, a further design optimisation was conducted, which resulted in a short-circuit tolerant optimised design shown in Fig. 8. The design parameters and the operating point results are summarised for this design in Tables IV and V respectively. It can be observed that the design has thicker magnets to ensure no demagnetisation occurs and a longer stator slot opening (parameter S_1), which contributes to the slot leakage inductance and hence the total leakage flux of the motor. From Table V, the demagnetisation margin for the magnets are shown to be well above the "knee" point at either operating point during standard operation. Further under a short-circuit condition the magnets are within the "knee" point of the demagnetisation curve, which will therefore avoid any magnet degradation. The short-circuit characteristic current is also seen to be 1.68 times the rated current at base speed.
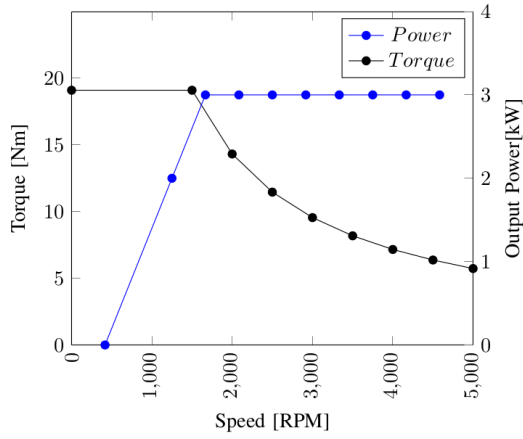
Fig. 9. Torque/power-speed characteristics of the final optimum design.

TABLE VI
INDUCTANCE CHARACTERISTICS.

Parameter	Initial Optimum Design	Final Design
L_s (μH)	834.51	850.14
L_m (μH)	436.29	292.65
L_l (μH)	398.22	557.49
L_σ (μH)	361.09	515.39
L_e (μH)	35.71	35.36
L_h (μH)	1.42	6.74
R_ϕ ($m\Omega$)	45.19	39.79

B. Analysis of inductance characteristics

From Section III, an increase in synchronous inductance leads to an improvement in the CPSR of a SPM motor. In Table VI the inductance characteristics are given, with L_e being the end winding inductance, L_h being the harmonic leakage inductance and R_ϕ being the terminal resistance. For the optimised short-circuit tolerant design, the magnetising inductance L_m and the leakage inductance L_L account for 34.42 % and 65.58 % of the total synchronous inductance, respectively, which shows the leakage inductance has a large contribution to the total synchronous inductance, which improves the flux weakening capability of the motor.

As given in Table VI, the slot leakage inductance L_σ is the biggest contributor to the synchronous leakage inductance when compared to the end-winding and harmonic leakage inductances. It can be clearly seen from the geometric layouts of the optimum designs (Figs. 7-8) that an extended parameter of S_1 and S_3 (see also Table IV) improves the slot leakage permeance factor (19), which in turn enhances flux weakening capability.

C. Costing, mass and efficiency

The cost and mass of each material used in the initial and short-circuit tolerant optimal motor designs are given in Table VII. From the optimisation, the short-circuit tolerant design was determined with a minimal increase to the total cost of the motor. As the PMs have the highest cost per kg, the optimisation determined a total PM mass of 0.173 kg for the short-circuit tolerant design, with the total mass of the

TABLE VII
DESIGN CHARACTERISTICS.

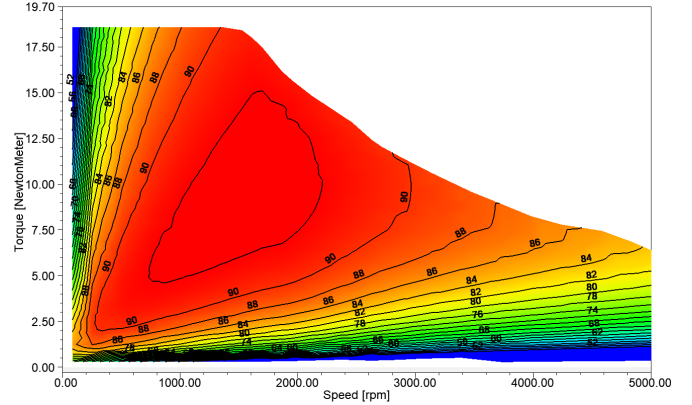| Parameter	Initial Optimum Design	Final Design
C_{total} (USD)	50.17	52.16
C_{steel} (USD)	23.02	22.19
C_{copper} (USD)	19.8	21.28
C_{magnet} (USD)	7.34	8.69
M_{total} (kg)	14.62	14.46
M_{steel} (kg)	11.42	11.1
M_{copper} (kg)	2.97	3.19
M_{magnet} (kg)	0.146	0.173
V_{total} (L)	2.02	2.04

Fig. 10. Efficiency map of the final optimum surface-mounted motor design.

motor being 14.46 kg. The total cost of the motor (based on the active material) is about 52.16 USD.

Figure 10 shows the efficiency map of the short-circuit tolerant optimised design. The efficiency map for the optimised design is generated assuming that the motor is always operated at maximum torque per ampere (MTPA). The total losses considered in the map includes the sum of resistive, core and eddy current losses. The motors mechanical losses are also considered, which was set to be 40 W at base speed. From this, the base speed efficiency is 91 %, while the maximum speed efficiency is 83 %. The flux density distribution at base and maximum speed is depicted in Fig. 11, which shows how the flux field is weakened when the motor operates at maximum speed, due to the significant synchronous inductance.
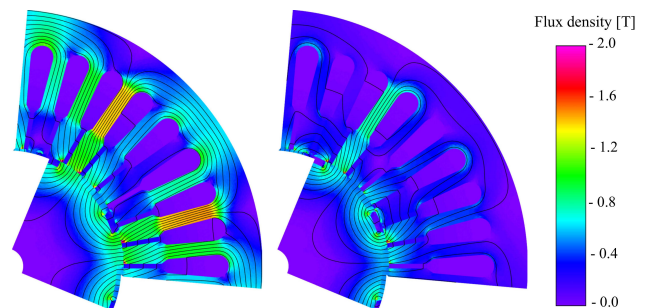

Fig. 11. Flux density distribution in the final optimum SPM motor design at 1500 r/min and 5000 r/min respectively.

VI. Conclusion

In this paper, a surface-mounted permanent magnet machine is designed using fractional-slot overlapping windings for a LEV. The motors parameters were designed to comply with certain specifications set for the LEV.

It was determined for a SPM design, in order to extend flux weakening capability, a large synchronous inductance is required. This can be accomplished by increasing the magnetising and slot leakage inductance. A multi-point design optimisation strategy was employed to search for the most cost-effective design, while ensuring a wide CPSR.

Furthermore, in this study it was found that the inverter sizing has a direct influence on the costing of the motor. As the size of the inverter was increased by $0.3\,\text{kVA}$, there was a reduction in motor cost by 52%. This shows that by allowing the inverter constraint to relax up to a point, a more cost effective machine can be realised without compromising significantly on the inverter's rating.

It was determined that the initial optimised design will experience magnet degradation under a short-circuit condition. Further design optimisation led to a final optimum design, which can withstand a dynamic short-circuit fault condition without demagnetising the magnets.

Lastly it was found that a surface-mounted SPM design with overlapping winding is able to achieve a wide CPSR without compromising on efficiency. This takes into account that no segmentation of magnets are employed, which may further increase the motor's efficiency.

References

[1] J. Yan, K. Yang, S. Zhang, Y. Feng, Y. Chen, and H. Yang, "Comparative investigation of inset-type and V-type IPMSM for light electric vehicle," *International Journal of Applied Electromagnetics and Mechanics*, vol. 54, no. 4, pp. 515–524, 2017.

[2] A. G. Sarigiannidis, M. E. Beniakar, and A. G. Kladas, "Fast adaptive evolutionary PM traction motor optimization based on electric vehicle drive cycle," *IEEE Transactions on Vehicular Technology*, vol. 66, no. 7, pp. 5762–5774, 2016.

[3] G. Pellegrino, A. Vagati, P. Guglielmi, and B. Boazzo, "Performance comparison between surface-mounted and interior PM motor drives for electric vehicle application," *IEEE Transactions on Industrial Electronics*, vol. 59, no. 2, pp. 803–811, 2011.

[4] K. M. Cissé, S. Hlioui, Y. Cheng, M. Belhadi, and M. Gabsi, "Optimization of V-shaped synchronous motor for automotive application," in *XIII International Conference on Electrical Machines (ICEM)*. IEEE, 2018, pp. 906–912.

[5] J. Wang, X. Yuan, and K. Atallah, "Design optimization of a surface-mounted permanent-magnet motor with concentrated windings for electric vehicle applications," *IEEE Transactions on Vehicular Technology*, vol. 62, no. 3, pp. 1053–1064, 2012.

[6] S. Pastellides, S. Gerber, and R.-J. Wang, "Design strategy and comparison of four PM motor topologies for a $2\,\text{kW}$ traction application," in *Southern African Universities Power Engineering Conference/Robotics and Mechatronics/Pattern Recognition Association of South Africa (SAUPEC/RobMech/PRASA)*. IEEE, 2019, pp. 358–363.

[7] R. Krishnan, *Permanent magnet synchronous and brushless DC motor drives*. CRC press, 2017.

[8] P. Ponomarev, P. Lindh, and J. Pyrhönen, "Effect of slot-and-pole combination on the leakage inductance and the performance of tooth-coil permanent-magnet synchronous machines," *IEEE Transactions on Industrial Electronics*, vol. 60, no. 10, pp. 4310–4317, 2012.

[9] A. M. El-Refaie and T. M. Jahns, "Optimal flux weakening in surface PM machines using fractional-slot concentrated windings," *IEEE Transactions on Industry Applications*, vol. 41, no. 3, pp. 790–800, 2005.

[10] A. M. El-Refaie and T. M. Jahns, "Impact of winding layer number and magnet type on synchronous surface PM machines designed for wide constant-power speed range operation," *IEEE Transactions on Energy Conversion*, vol. 23, no. 1, pp. 53–60, March 2008.

[11] Y. Duan, R. Harley, and T. Habetler, "Method for multi-objective optimized designs of surface mount permanent magnet motors with concentrated or distributed stator windings," in *IEEE International Electric Machines and Drives Conference*. IEEE, 2009, pp. 323–328.

[12] G. Dajaku and D. Gerling, "A novel tooth concentrated winding with low space harmonic contents," in *International Electric Machines & Drives Conference*. IEEE, 2013, pp. 755–760.

[13] K. T. Chau, *Electric vehicle machines and drives*. Wiley, 2015.

[14] M. Ehsani, Y. Gao, S. Longo, and K. Ebrahimi, *Modern electric, hybrid electric, and fuel cell vehicles*. CRC press, 2018.

[15] H. Liu, Z. Zhu, E. Mohamed, Y. Fu, and X. Qi, "Flux-weakening control of nonsalient pole PMSM having large winding inductance, accounting for resistive voltage drop and inverter nonlinearities," *IEEE Transactions on Power Electronics*, vol. 27, no. 2, pp. 942–952, 2011.

[16] J. F. Gieras, *Permanent magnet motor technology: design and applications*. CRC press, 2009.

[17] S.-K. Sul, *Control of electric machine drive systems*. John Wiley & Sons, 2011.

[18] W. Gu, X. Zhu, L. Quan, and Y. Du, "Design and optimization of permanent magnet brushless machines for electric vehicle applications," *Energies*, vol. 8, no. 12, pp. 13 996–14 008, 2015.

[19] J. Pyrhonen, T. Jokinen, and V. Hrabovcova, *Design of rotating electrical machines*, 2nd ed. Wiley, 2014.

[20] D. Kraft and K. Schnepper, "SLSQP—a nonlinear programming method with quadratic programming subproblems," *DLR, Oberpfaffenhofen*, 1989.

[21] P. M. Tlali, R.-J. Wang, S. Gerber, C. D. Botha, and M. J. Kamper, "Design and performance comparison of vernier and conventional PM synchronous wind generators," *IEEE Transactions on Industry Applications*, vol. 56, no. 3, pp. 2570–2579, 2020.

[22] J. Germishuizen and C. Adam, "Integrating FEM and existing traction motor design tools into an everyday engineering environment," *e & i Elektrotechnik und Informationstechnik*, vol. 136, no. 2, pp. 168–174, 2019.

VII. Biographies

Stavros Pastellides received his B.Eng in Electrical Engineering at Stellenbosch University in 2017 where he is currently working as a Masters researcher. His main interests are electrical machine design, numerical optimization, electric vehicle traction drive systems and renewable energy systems.

Stiaan Gerber received his Ph.D. in Electrical Engineering at Stellenbosch University in 2015 where he is currently working as a postdoctoral researcher. His main interests in the engineering field are electrical machine design, magnetic gear technology, numerical optimization, finite element methods and renewable power generation. He is an avid software developer and has published more than 20 papers in recognized international journals and conference proceedings.

Rong-Jie Wang received the M.Sc. degree in electrical engineering from the University of Cape Town in 1998 and the Ph.D. degree in electrical engineering from Stellenbosch University in 2003, all in South Africa. He is currently an Associate Professor in the Department of Electrical and Electronic Engineering at Stellenbosch university. His research interests include novel topologies of permanent magnet machines, computer-aided design and optimization of electrical machines, cooling design and analysis, and renewable energy systems.

Maarten Kamper received the M.Sc. (Eng.) and Ph.D. (Eng.) degrees from the Stellenbosch University in South Africa, in 1987 and 1996, respectively, in the field of design of induction and reluctance electrical machines. Since 1989, he has been with the Department of Electrical and Electronic Engineering, Stellenbosch University, where he is currently a Professor of electrical machines and drives. His research interests include the design optimization and control of electrical machines, currently with the focus on wind generators, synchronous condensers and industrial and electric vehicle drives. Prof Kamper is a senior member of the IEEE and a registered professional engineer in South Africa.